Excitation-autoionization cross sections and rate coefficients of Zn-like ions

D. Mitnik, P. Mandelbaum, and J. L. Schwob
Racah Institute of Physics, The Hebrew University, 91904 Jerusalem, Israel

A. Bar-Shalom and J. Oreg
Nuclear Research Center–Negev, P.O. Box 9001, 84190 Beer Sheva, Israel
(Received 15 July 1996)

Detailed level-by-level calculations of the excitation-autoionization (EA) cross sections and rate coefficients were performed using the relativistic distorted-wave method along the Zn isoelectronic sequence for all the elements with $34 \leqslant Z \leqslant 92$. While in a previous work only the $3d$-$4l$ inner-shell collisional excitations were taken into account, the present calculations also include excitations to higher configurations: $3d^9 4s^2 nl$ ($n=4$ to 7) and $3p^5 3d^{10} 4s^2 nl$ ($n=4,5$). An extrapolation method is used to evaluate the total contribution for the higher principal quantum numbers. Configuration mixing and secondary autoionization processes following radiative decay from autoionizing levels are also included. The results show that the total EA rate is dominant compared to the direct ionization rate, up to a factor 12 at $Z=47$. The additional inner-shell excitations for $Z<59$ produce an increase in the EA effect varying from 25% to almost a factor of 2, with respect to the previously predicted EA effect through $3d$-$4l$ only. The excitations to the higher configurations are the most significant for heavy elements with $Z \geqslant 61$, since they open EA channels, resulting in an EA rate which varies along the sequence from 4 to 1 times the direct-ionization rate. [S1050-2947(96)08012-2]

PACS number(s): 32.80.Dz, 34.80.Dp, 34.80.Kw, 52.25.Kn

I. INTRODUCTION

The excitation-autoionization (EA) process, which consists of collisional excitation to a level above the ionization limit followed by autoionization, is an important indirect ionization mechanism for charged atoms. In particular, EA can significantly alter the ionization balance in hot plasmas. This process has been thoroughly investigated for ions isoelectronic to light elements, and most of those works can be found, for instance, in comprehensive reviews [1–3]. In contrast, rather few data are available for more complex ions, especially for heavy ionized atoms belonging to the sequences isoelectronic to the fourth-row elements with $3d^{10} 4s^x 4p^y$ ($x=1,2$ and $y=0$–6) ground states.

The present work is a continuation of a systematic investigation of EA for ions in these sequences. In a previous work we computed the EA rate coefficients for all the sequences from CuI to KrI, but including only the most important $3d$-$4l$ inner-shell excitations [4]. The EA processes are particularly important for these sequences, due to the presence of the ten $3d$ inner-shell electrons. It was shown that these processes have a significant effect on the ionization balance in coronal plasma conditions, lowering the temperature of maximum fractional ion abundances by as much as 40%. In some cases the EA rates exceed the direct-ionization rates by up to one order of magnitude. The $3d$-$4l$ EA channels increase the total ionization rate mostly for light or moderate heavy elements, since as Z increases the $3d$-$4l$ inner-shell excited configurations fall below the ionization limit and cease to be autoionizing. Therefore, in order to obtain accurate total EA cross sections and rate coefficients the calculations have to be extended to include the other excitation channels. In a recent work on the Cu sequence [5] we showed that excitations to *higher* inner-shell excited configurations can enhance the EA rate by up to a factor of 2 for $Z \leqslant 54$, and open EA channels for the heavy elements ($Z>55$).

In the present work we investigate this effect for the Zn isoelectronic sequence, and calculate the *total* EA contribution along the whole sequence. The present revised calculations include, in addition to the $3d^9 4s^2 4l$ configurations which were taken into account in Ref. [4], the *higher* inner-shell excited configurations: $3d^9 4s^2 nl$ ($n=5$ to 7; $l=0$ to $n-1$) and $3p^5 3d^{10} 4s^2 nl$ ($n=4,5$; $l \leqslant n-1$). Moreover, an extrapolation method is used to evaluate the contribution of the even higher-lying configurations. All these additional contributions are important in the Zn sequence too, since the $3d^9 4s^2 4l$ configuration complex falls below the ionization limit already for $Z=61$, and thus for heavier elements excitations to the higher configurations constitute the only EA channels. Configuration mixing and further autoionization following radiative decays are included in the present revised calculations. Finally, since the Zn-like ions can have significantly populated metastable levels, EA processes from these levels may turn out to be important and are also calculated here. The contribution of these levels to the total EA effect will be discussed.

II. THEORETICAL METHODS

The theoretical method is similar to that described in detail in a preceding work on EA along the Cu sequence [5]. One assumes that the only important collisional processes are electron-impact excitation and ionization from the ground state. The total cross section σ_C^{EA} for excitation-autoionization from the ground configuration g ($3p^6 3d^{10} 4s^2$) of a Zn-like ion, to any final level k of the Cu-like ion, through inner-shell excitation of the Zn-like ion to any intermediate autoionizing level j within a given configuration or complex C (of the Zn-like ions) is given by

$$\sigma_C^{EA}(E)=\sum_{j\in C}\sigma_{gj}(E)\left[\frac{\Sigma_k A_{jk}^a+\Sigma_i A_{ji}B_i^a}{\Sigma_k A_{jk}^a+\Sigma_i A_{ji}}\right]\equiv\sum_{j\in C}\sigma_{gj}(E)B_j^a\,, \tag{1}$$

where $\sigma_{gj}(E)$ is the cross section for electron-impact excitation from g to j as a function of the incident electron kinetic energy E. A_{jk}^a is the rate coefficient for autoionization from j to k and A_{ji} is the Einstein coefficient for spontaneous emission from j to any lower-lying level i.

B_j^a is the *multiple* or *effective branching ratio for autoionization* from level j, defined by the bracket term. This term contains in turn the effective branching ratio B_i^a for further (secondary) autoionization from level i, defined by a similar recursive expression (see Ref. [5]). This model allows one to take into account all the possible secondary autoionizations following cascading, until the ion reaches via radiative decay a level m below the first ionization limit ($B_m^a=0$).

In our previous work on the Cu isoelectronic sequence, the impact of the multiple-autoionization branching ratio approach has been investigated by comparison to two simple models: the usual model assuming $B_i^a=0$, and the opposite approximation $B_i^a=1$. The conclusion was that the latter model represents a poor approximation, leading to high overestimations for high-Z elements, whereas the first approximation leads to an error of less than 2%. In this work we will compare the results for the Zn sequence also to those obtained using the usual $B_i^a=0$ approximation. In addition, here we introduce for comparison another even simpler model in which $B_i^a=0$ also, but among all the radiative decays represented in the ΣA_{ji} sum in the denominator of expression (1) only those to levels lying *below* the first ionization limit are taken into account. This approximation was proved to give fairly good results in dielectronic recombination calculations by Behar *et al.* [6]. Our purpose is to test the validity of this approximation for the EA calculations, since it could be attractive for use in more complex isoelectronic sequences (GeI to KrI), which involve an even larger number of levels.

The present level-by-level calculations are performed following the same computational methods used in previous works [4,5]. These are based on the HULLAC (Hebrew University Lawrence Livermore Atomic Code) computer package; this includes the computer code RELAC (Relativistic Parametric Potential Atomic Code) for atomic energy level and radiative transition rate calculations [7], which has been extended to calculate the autoionization rates following the distorted-wave (DW) approximation [8]. The electron-impact excitation cross sections and rate coefficients are calculated in the DW approximation using the CROSS code [9] which is based on the factorization interpolation method.

Our calculations do not include resonant-excitation double-autoionization (REDA) processes [10]. Including these processes would lead to extremely difficult calculations due to the large number of configurations to be included and their complex structures.

Both EA cross sections and rate coefficients have been calculated. The rate coefficient S_C^{EA} for excitation-autoionization (through a given configuration C) as a function of the electron temperature T_e is given by

$$S_C^{EA}=\int_0^\infty v f(v)\sigma_C^{EA}(v)dv=\sum_{j\in C}Q_{gj}B_j^a\,, \tag{2}$$

where v is the electron velocity and $f(v)$ is the electron velocity distribution (assumed Maxwellian). Q_{gj} is the electron-impact excitation rate coefficient from the ground level g to level j. The results presented here are limited to elements with $Z\geqslant 34$, since for low ionization stages the calculation method becomes less accurate.

III. CALCULATIONAL PROCEDURE

A. $3d$-nl ($4\leqslant n\leqslant 7$) inner-shell excitations

The main inner-shell collisional excitations involved in the EA processes are the $3d$-$4l$ excitations, already studied in our previous work [4]. The calculations for these main EA processes include excitations to all the 286 levels of the $3d^9 4s^2 4l$ ($l=d,f$) configurations, which are directly excited from the ground state ($3d^{10}4s^2$). The model also includes the configurations that could produce configuration mixing effects [11]: $3d^9 4s 4p^2$ (which mixes strongly with $3d^9 4s^2 4d$) and $3d^9 4s 4p 4d$ (which mixes with $3d^9 4s^2 4f$). In the Zn sequence, the effect of configuration mixing can be especially significant due to the fact that the ground state is a closed-shell state with $J=0$ [4]. All electric-dipole allowed radiative decays are considered, i.e., transitions to the ground state and to the low configurations $3d^{10}4s4l$ ($l=p,d$), as well as to the inner-shell excited configurations $3d^9 4s^2 4p$ (which lie below the first ionization limit for all the ions considered here) and to $3d^9 4s^2 4d$. Autoionization processes to the $3d^{10}4s$, $3d^{10}4p$ and $3d^{10}4d$ Cu-like levels are taken into account.

In the present revised calculations we have taken into account the following additional configuration interactions for the $3d$-$4l$ excitations: $3d^9 4s^2 4d + 3d^9 4s^2 5d$ and $3d^9 4s^2 4f + 3d^9 4s^2 5f$. Furthermore, in addition to the sole $3d$-$4l$ excitations considered in the previous work, the calculations now include the $3d$-nl ($5\leqslant n\leqslant 7$) inner-shell excitations, involving the configurations $3d^9 4s^2 nl$ ($l=0$ to $n-1$). In fact, the $3d^9 4s^2 7i$ configuration gives a negligible contribution, and we have not taken it into account. As will be discussed in Sec. IV, these $3d$-nl ($n\geqslant 5$) excitations have been calculated neglecting interactions between configurations with different principal quantum numbers. For the radiative decays, all the relevant lower configurations are taken into account: $3d^{10}4s^2$, $3d^9 4s^2 n'l'$ ($n'\leqslant n$, $l'=0$ to $n'-1$), $3d^9 4s 4p^2$ and $3d^9 4s 4p 4d$. This implies radiative transitions to lower autoionizing inner-shell excited configurations. In all the present calculations we have taken possible secondary autoionization processes into account by introducing the multiple branching ratio factor B_i^a. Autoionization processes from the $3d^9 4s^2 nl$ configurations with $n>4$ are possible only to the ground state $3d^{10}4s$ of the Cu-like ions.

B. $3p$-nl ($n=4,5$) inner-shell excitations

In addition to the $3d$-nl excitations, the present detailed calculations include the $3p$-nl inner-shell excitations. The $3p$-$4l$ excitations involve the $3p^5 3d^{10}4s^2 4l$ ($l=p,d,f$) configurations. We have taken into account the most important

configuration mixings: $3p^5 3d^{10}[4s^2 4d + 4s4p^2]$ and $3p^5 3d^{10}[4s^2 4f + 4s4p4d]$. The radiative decays considered are to the ground state and to the following low-lying configurations: $3p^6 3d^{10} 4s4l$ $(l=p,d,f)$, $3p^6 3d^{10} 4p4l$ $(l=p,d)$ and $3p^6 3d^9 4s^2 4l$ $(l=p,d,f)$ (including the configurations $3p^6 3d^9 4s4p^2$ and $3p^6 3d^9 4s4p4d$ which mix with them). The model includes autoionization processes to the $3d^{10}4l$ $(l=s,p,d,f)$ levels of the Cu-like ion.

The $3p$-$5l$ inner-shell excitations included in our calculations are to the $3p^5 3d^{10} 4s^2 5l$ $(l=s,p,d,f,g)$ configurations. For the radiative decays, all the relevant lower configurations are taken into account: $3p^6 3d^{10} 4s^2$, $3p^6 3d^{10} 4s5l$ $(l=s,p,d,f,g)$, $3p^6 3d^9 4s^2 5l$ $(l=s,p,d,f,g)$ and $3p^5 3d^{10} 4s^2 4l$ $(l=p,d,f)$ (including the corresponding mixing with $3p^5 3d^{10} 4s4p^2$ and $3p^5 3d^{10} 4s4p4d$). The model, which includes the radiative transitions to lower autoionizing levels, takes further possible autoionization from these levels into account, as for the $3d$-nl excitations considered above.

Unlike the case of the Cu isoelectronic sequence, in which autoionization from $3p$-nl inner-shell excited levels are energetically allowed mostly to the Ni-like $3d^{10}$ ground state, in the Zn sequence autoionization processes from $3p^5 3d^{10} 4s^2 nl$ to the $3d^{10}nl$ excited Cu-like levels may also be allowed in a part of the sequence, and therefore these processes are also taken into account. Due to the progressive decrease of the energies of the Zn-like $3p$-nl inner-shell excited configurations to below the $3d^{10}nl$ Cu-like levels as Z increases, one expects discontinuities in the EA effect along the isoelectronic sequence.

C. Extrapolation to higher configurations

In order to evaluate the rate coefficients for EA through the higher inner-shell configurations, an extrapolation procedure similar to that used for the Cu isoelectronic sequence has been used. In the Zn sequence, the EA contributions of the high-lying configurations also decrease as the principal quantum number n increases, in spite of the increasing number of EA channels. It is thus possible to extrapolate all the contributions up to $n \to \infty$.

Regarding first the $3d$-nl inner-shell excitations, for low n values $(4 \leqslant n \leqslant 7)$, the results of the detailed calculations show that among all the possible excitations the dominant ones are $3d$-nd and $3d$-nf. Here, we have found the same important property which was observed for the Cu-like ions: for low n numbers the results of the calculations show that the ratios of the EA contribution of $3d$-nd on one hand, and of $3d$-nf on the other hand, to the *total* $3d$-nl EA rate coefficients are almost independent of n. This property is important since it can lead to a substantial reduction in the amount of calculations. The ratios vary slightly and smoothly as a function of Z. Consequently, an analytical extrapolation is only needed for the two excitations $3d$-nd and $3d$-nf as a function of n.

In order to evaluate the asymptotic form of $S^{EA}(n)$ for high quantum numbers n, we have performed the extrapolation on n independently for the collisional excitation rate coefficient Q and for the branching ratio for autoionization B^a. The total $3d$-nd and $3d$-nf excitation rate coefficients have been obtained using detailed DW calculations for n up to 15. The results were introduced to get a best fit of the parameters in the Van Regemorter approximate formula [12]. Indeed, this expression is an analytical function of the temperature and of the level energy which can be expressed in terms of the hydrogenic asymptotic expression as a function of n. On the other hand, the averaged autoionization branching ratios are calculated for the $3d^9 4s^2 nd$ and $3d^9 4s^2 nf$ configurations from $n=4$ to 7. The results show a systematic decrease of the branching ratios along the whole isoelectronic sequence. However, a direct extrapolation of the autoionization branching ratios on the basis of these results obtained for relatively low n numbers is not accurate enough. Thus, the extrapolation has been done independently for the autoionization coefficients A^a and for the radiative Einstein coefficients A. A detailed analysis of the results for up to $n=15$ enables us to obtain asymptotic functions of n and Z for both A^a and A. For the same reasons explained in our previous paper [5], the autoionization branching ratios decrease as a function of n (instead of the pure hydrogenic asymptotic behavior which tends to 1).

A similar procedure has been applied in order to extrapolate the EA contributions of the $3p$-nl $(n=6$ to $\infty)$ inner-shell excitations. The calculations in this case show some differences compared to the Cu isoelectronic sequence. First, the contributions of the $3p$-nf and $3p$-nd transitions are important (specially for low-Z elements), and therefore not only the dominant $3p$-np transitions have to be taken into account. Second, the $3p$-nl EA rate coefficients are no longer smooth functions of Z. As indicated above (Sec. III B), it is now necessary to include the additional autoionizing channels towards the excited Cu-like configurations $3d^{10}nl$ in the calculations. Therefore, the progressive decrease of the Zn-like $3p^5 3d^{10} 4s^2 nl$ inner-shell excited levels to below the Cu-like $3d^{10}nl$ levels as Z increases plays an important role. In fact, one can consider these two complexes as two Rydberg series tending asymptotically to the $3p^5 3d^{10} 4s^2$ and $3d^{10}$ parent configurations of the Cu- and Ni-like ions, respectively, as n increases. The Cu-like $3p^5 3d^{10} 4s^2$ configuration consists of two levels, ($J=3/2$ and $J=1/2$). The lower $3p^5 3d^{10} 4s^2$ $[J=3/2]$ level falls below the first ionization limit ($3d^{10}$ Ni-like ground state) already for $Z \geqslant 53$, whereas the higher level $[J=1/2]$ lies below $3d^{10}$ only for $Z \geqslant 63$. The Zn-like $3p^5 3d^{10} 4s^2 nl$ and the Cu-like $3d^{10}nl$ configurations consist mainly of two groups of levels, and their respective positions follow a behavior similar to the parent configurations. In fact, level-by-level calculations have shown that the lower level group of $3p^5 3d^{10} 4s^2 nl$ falls below $3d^{10}nl$ at $Z=53$ for very large n, but at slightly higher Z for low n: for $n=6$ this occurs at $Z \geqslant 55$. On the other hand, the higher level group falls below $3d^{10}nl$ at $Z=63$ for $n>12$, whereas this group is still above $3d^{10}nl$ for lower n values. Only at $Z \geqslant 70$, are both level groups completely below this ionization limit for all n values $(n \geqslant 5)$. Accordingly, we have derived two different n-dependence functions for extrapolating the autoionization rate coefficients of the $3p^5 3d^{10} 4s^2 nl$ configurations, depending on whether Z is lower than 53, or higher than 70. In the intermediate Z range a smooth quasilinear interpolation between the two $A^a(n)$ branches has been made. One notices that the dominant radiative transitions from the $3p^5 3d^{10} 4s^2 nl$ configurations are the $4s \to 3p$ and the

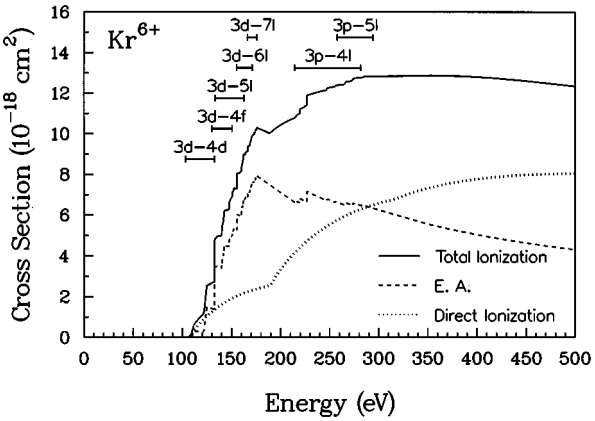

FIG. 1. Calculated direct-ionization cross section, total EA cross section, and total (EA+direct) ionization cross section as a function of the incident electron energy, for Kr^{6+}. The energy domains of the various inner-shell transitions are indicated above the curves.

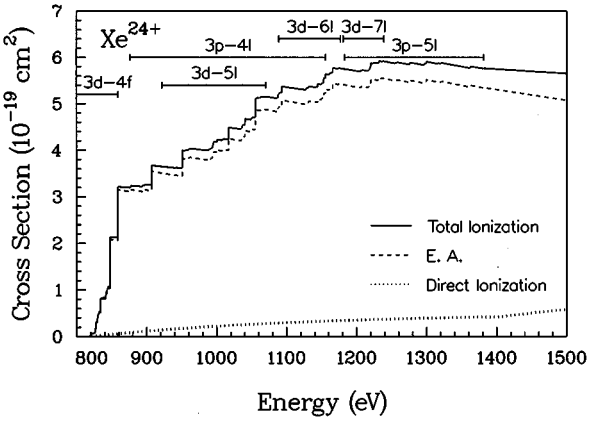

FIG. 3. Calculated direct-ionization cross section, total EA cross section, and total (EA+direct) ionization cross section, for Xe^{24+}. The energy domains of the various inner-shell transitions are indicated above the curves.

$3d \rightarrow 3p$ transitions, and their radiative coefficients A are independent of the principal quantum number n of the spectator electron. Therefore, the autoionization rates are those which mainly dictate the final behavior of the autoionization branching ratios as a function of the quantum number n.

IV. RESULTS

A. EA cross section

Figures 1 to 5 display the results of the total electron-impact EA cross sections calculated for several Zn-like ions: Kr^{6+} ($Z=36$), Mo^{12+} ($Z=42$), Xe^{24+} ($Z=54$), Pr^{29+} ($Z=59$), and Dy^{36+} ($Z=66$). These results are obtained through the level-by-level calculations involving 804 inner-shell excited levels which correspond to the following inner-shell excitations: $3d$-$4l$, $3d$-$5l$, $3d$-$6l$, $3d$-$7l$, $3p$-$4l$, and $3p$-$5l$ (the extrapolated contributions from higher configurations are not included in the figures). In these figures we also show the direct-ionization and the total (EA+direct) ionization cross sections. The direct-ionization cross section is calculated using the simple approximate Lotz formula [13], although it is generally recognized to lead to a slight overestimation.

The main peaks in the excitation-autoionization cross section curves for these Zn-like ions are listed in Table I. The first column gives the transitions between the ground-state and the inner-shell excited configurations to which the peak belongs. The second column displays the incident electron energy of the peak, i.e., the energy threshold for the excitation to the inner-shell excited level which gives the highest EA contribution within the whole configuration. The EA contribution for the *whole configuration* at this energy is given in the next column. The last column displays the value of the *total* EA cross section at the same energy. The energy domains of the various inner-shell transitions are indicated above the cross-sections curves in Figs. 1 to 5. For Kr^{6+} a theoretical EA cross section has been published by Gorczyca *et al.* [14]. The present EA results are in fairly good agreement with these data. The values of the total EA cross section obtained in the present calculations are about 10%

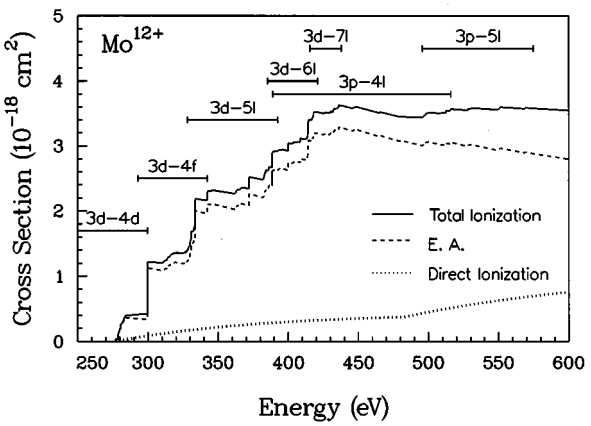

FIG. 2. Calculated direct-ionization cross section, total EA cross section, and total (EA+direct) ionization cross section, for Mo^{12+}. The energy domains of the various inner-shell transitions are indicated above the curves.

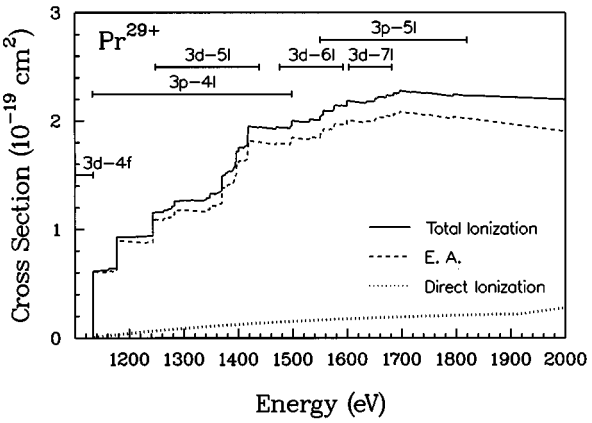

FIG. 4. Calculated direct-ionization cross section, total EA cross section, and total (EA+direct) ionization cross section, for Pr^{29+}. The energy domains of the various inner-shell transitions are indicated above the curves.

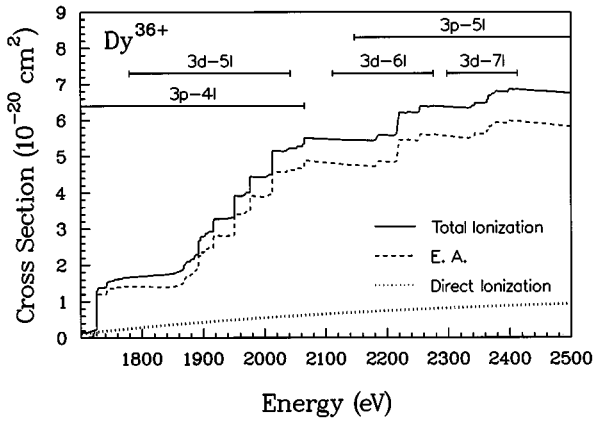

FIG. 5. Calculated direct-ionization cross section, total EA cross section, and total (EA+direct) ionization cross section, for Dy^{36+}. The energy domains of the various inner-shell transitions are indicated above the curves.

higher in the low-energy range. At high energies the discrepancy is a little higher due to the contribution of the $3p$-nl excitations not included in the calculations by Gorczyca *et al.*

It is worth noting that regarding the $3d$-$4d$ excitation cross sections, the main contribution comes from the excitation to the highest level $3d_{5/2}^9 4s^2 4d_{5/2}$ $[J=0]$ ($^1S_0$ in LS coupling). This level has a particularly strong repulsive exchange potential, and therefore corresponds to a larger orbit radius than the other levels of the configuration. This level is thus poorly described by minimizing the potential parameters for the whole configuration, and consequently it can cause a large error in this particular excitation cross section. According to a previous work [5], one way to partially correct this term dependence problem is to allow configuration mixing between the $3d^9 4s^2 4d$ and $3d^9 4s^2 5d$ configurations ($[4d+5d]$), so that the $4d$ orbital for the $^1S_0$ level is now represented by a weighted sum of the $4d$ and $5d$ wave functions. Thus, in the present calculations we have followed this procedure, by calculating the $3d$-$4d$ EA cross sections including the $[4d+5d]$ configuration mixing. The addition of configuration mixing with $3d^9 4s^2 nd$ with $n>5$ is found to lead to a very small change. In summary, for the $3d$-$4l$ excitations taking into account the effect of mixing between configurations with different principal quantum numbers n but the same l leads to a decrease of the computed $S_{3d\text{-}4l}^{EA}$ of about 25% in the case of Kr^{6+}. As already noticed in the Cu sequence, the effect of this kind of mixing becomes smaller as Z increases.

Regarding the $3d$-$5d$ excitations, including only the $[4d$-$5d]$ mixing causes a large error in the calculated cross section for the excitation to the $3d^9 4s^2 5d$ configuration, and especially to the dominant $^1S_0$ level. As for the Cu-like ions, in order to correct this inaccuracy, it would be necessary to include further configuration mixing with higher nd configurations. However, we have found that the results obtained for the $3d$-$5d$ excitations without any mixing at all with $3d^9 4s^2 nd$ configurations, are close enough to the asymptotic values obtained by using the full $[4d+5d+6d+7d+8d+\cdots]$ mixing. The approximation of isolated configurations (with different n) is even more accurate for the $3d$-nd excitations with $n>5$.

We have proceeded similarly for the $3d$-nf excitations. Only the $[4f+5f]$ configuration mixing has been included for the $3d$-$4f$ excitation cross sections; but again for the $3d$-nf ($n\geqslant 5$) excitations the results obtained using the isolated configuration approximation are found to be accurate enough and are given here.

B. Total EA rate coefficients

The total excitation-autoionization rate coefficients S^{EA}, computed through level-by-level calculations involving the inner-shell excitations $3d$-nl ($n=4$ to 7) and $3p$-nl ($n=4$ and 5), and including the extrapolated EA contributions for higher n numbers, are given in Table II. The results are presented for all the elements ($34\leqslant Z\leqslant 92$) in the electron temperature range $0.1E_I\leqslant kT_e\leqslant 10E_I$, where E_I is the first ionization limit.

In order to show the contributions to the ionization enhancement due to the various EA channels, the ratios between S_C^{EA} for excitation-autoionization through the different configuration complexes and the direct-ionization rate coefficient S (at $kT_e=E_I$) are shown in Figs. 6 and 7, together with the ratio between the total EA rate coefficient S^{EA} and S.

For elements having $Z\leqslant 60$ the most important contribution to EA is through $3d$-$4d$ and $3d$-$4f$ inner-shell excitations (Fig. 6). At low Z, the autoionizing configurations $3d^9 4s^2 4d$ and $3d^9 4s^2 4f$ are relatively high with respect to the first ionization limit. For $34\leqslant Z\leqslant 47$ the ratio S^{EA}/S increases as a function of Z. This is due to the fact that the energies of the $3d^9 4s^2 4d$ and $3d^9 4s^2 4f$ autoionizing levels decrease progressively as Z increases, while still remaining above the ionization limit, thus favoring the inner-shell excitation processes more and more. The first abrupt decrease in S^{EA}/S occurs at $Z=48$ and is due to the fall of the $3d_{5/2}^9 4s^2 4d_{5/2}$ $[J=0]$ level below the first ionization limit. For higher Z the main EA contribution is then due to the inner-shell excitations from the ground state to the $3d^9 4s^2 4f$ configuration, which are dominated by a few levels; thus one observes the successive closing of the autoionization channels as Z further increases up to $Z=61$, for which the $3d^9 4s^2 4f$ channels are completely closed.

The next important contributions, are given by $3p$-$4l$ and $3d$-$5l$ inner-shell excitations, which play the main role for ions having $Z\geqslant 61$. Among the first group, the dominant transition is $3p$-$4p$, which gives a maximum EA contribution at $Z=64$ (Fig. 7). At $Z=65$ one of the main $3p$-$4p$ excited levels falls below the first ionization limit; this leads to a noticeable drop of the EA rate. The $3p$-$4p$ EA channel is almost completely closed at $Z=82$. The other $3p$-$4l$ inner-shell excited autoionizing levels give a S_C^{EA} rate coefficient (at $kT_e=E_I$) from about 50% of the direct-ionization rate coefficient S at $Z=65$, to about 15% at $Z=80$. All the $3p^5 3d^{10} 4s^2 4l$ inner-shell excited configurations still have a few levels lying above the first ionization limit for all the ions ($Z\leqslant 92$). However, their contribution to the ionization enhancement becomes negligible for elements with $Z\geqslant 86$.

The contribution of the $3d$-$5l$ excitations to the total ionization rates is shown in Fig. 6. The ratio S_C^{EA}/S (at

TABLE I. Main contributions to the excitation-autoionization cross section, for Kr^{6+}, Mo^{12+}, Xe^{24+}, Pr^{29+}, and Dy^{36+}. The first column gives the inner-shell configuration transition to which the main EA peak belongs. The second column displays the incident electron energy threshold for the excitation to the level corresponding to the EA peak. The EA contribution for the whole configuration transition and the total EA cross section at this energy are given in the third and fourth columns, respectively. $X[-Y]$ means $X\times10^{-Y}$.

Transition	Excitation energy (eV)	EA cross section σ_C^{EA} (cm^2)	Total EA cross section σ^{EA} (cm^2)
	(a) Kr^{6+}, E_I=107.0 eV		
$3d\rightarrow4d$	124.7	1.50[-18]	1.50[-18]
$3d\rightarrow4d$	132.6	3.41[-18]	3.41[-18]
$3d\rightarrow4f$	150.7	1.49[-18]	4.98[-18]
$3d\rightarrow5d$	155.7	1.18[-18]	6.03[-18]
$3d\rightarrow5f$	162.0	8.35[-19]	6.82[-18]
$3d\rightarrow6d$	166.6	4.99[-19]	7.16[-18]
$3d\rightarrow6f$	170.4	4.65[-19]	7.57[-18]
$3d\rightarrow7d$	173.1	2.61[-19]	7.73[-18]
$3d\rightarrow7f$	175.5	2.83[-19]	7.93[-18]
$3p\rightarrow4p$	227.1	8.58[-19]	7.16[-18]
$3p\rightarrow5p$	266.3	1.05[-19]	6.61[-18]
	(b) Mo^{12+}, E_I=276.6 eV		
$3d\rightarrow4d$	299.6	1.13[-18]	1.13[-18]
$3d\rightarrow4f$	333.6	9.64[-19]	1.98[-18]
$3d\rightarrow4f$	342.2	1.09[-18]	2.09[-18]
$3d\rightarrow5d$	372.1	2.92[-19]	2.26[-18]
$3d\rightarrow5f$	388.6	4.40[-19]	2.61[-18]
$3p\rightarrow4p$	400.0	1.70[-19]	2.74[-18]
$3d\rightarrow6d$	408.6	1.14[-19]	2.81[-18]
$3p\rightarrow4p$	414.2	3.92[-19]	3.06[-18]
$3d\rightarrow6f$	418.0	2.17[-19]	3.20[-18]
$3d\rightarrow7f$	435.9	1.22[-19]	3.29[-18]
$3p\rightarrow5p$	512.5	4.55[-20]	3.04[-18]
	(c) Xe^{24+}, E_I=817.8 eV		
$3d\rightarrow4f$	847.5	2.09[-19]	2.09[-19]
$3d\rightarrow4f$	859.1	3.15[-19]	3.15[-19]
$3p\rightarrow4p$	906.8	5.18[-20]	3.55[-19]
$3p\rightarrow4p$	950.6	8.84[-20]	3.82[-19]
$3d\rightarrow5d$	1016.9	3.94[-20]	4.25[-19]
$3d\rightarrow5f$	1055.3	6.66[-20]	4.82[-19]
$3p\rightarrow4f$	1093.0	3.33[-20]	5.08[-19]
$3d\rightarrow6d$	1144.5	1.42[-20]	5.10[-19]
$3d\rightarrow6f$	1165.8	2.42[-20]	5.44[-19]
$3d\rightarrow7f$	1232.1	1.19[-20]	5.56[-19]
$3p\rightarrow5p$	1281.0	1.45[-20]	5.49[-19]
	(d) Pr^{29+}, E_I=1124.2 eV		
$3d\rightarrow4f$	1133.7	5.95[-20]	6.09[-20]
$3p\rightarrow4p$	1176.5	3.10[-20]	8.97[-20]
$3p\rightarrow4p$	1243.1	5.13[-20]	1.09[-19]
$3d\rightarrow5d$	1369.8	2.09[-20]	1.37[-19]
$3d\rightarrow5f$	1417.9	3.16[-20]	1.82[-19]
$3p\rightarrow4f$	1498.1	2.27[-20]	1.85[-19]
$3d\rightarrow4d$	1550.1	7.06[-21]	1.88[-19]
$3d\rightarrow6f$	1576.7	1.09[-20]	1.97[-19]
$3p\rightarrow5p$	1599.5	5.22[-21]	2.01[-19]
$3d\rightarrow7d$	1656.0	3.34[-21]	2.03[-19]

TABLE I. (*Continued*).

Transition	Excitation energy (eV)	EA cross section σ_C^{EA} (cm^2)	Total EA cross section σ^{EA} (cm^2)
$3d\rightarrow 7f$	1672.1	5.22[-21]	2.05[-19]
	(e) Dy^{36+}, $E_I=1637.6$ eV		
$3p\rightarrow 4p$	1726.1	1.07[-20]	1.13[-20]
$3p\rightarrow 4f$	1895.2	9.57[-21]	2.36[-20]
$3p\rightarrow 4d$	1917.5	4.81[-21]	2.82[-20]
$3d\rightarrow 5d$	1950.3	9.81[-21]	3.42[-20]
$3d\rightarrow 5f$	1976.2	5.37[-21]	3.92[-20]
$3d\rightarrow 5f$	2012.6	1.24[-20]	4.59[-20]
$3p\rightarrow 4f$	2053.5	1.04[-20]	4.67[-20]
$3p\rightarrow 5p$	2217.6	2.72[-21]	5.13[-20]
$3d\rightarrow 6d$	2220.0	3.23[-21]	5.46[-20]
$3d\rightarrow 6f$	2254.4	4.01[-21]	5.61[-20]
$3d\rightarrow 7d$	2378.3	1.49[-21]	5.94[-20]
$3d\rightarrow 7f$	2399.2	1.85[-21]	5.99[-20]

$kT_e=E_I$) increases from 0.2 to 0.7 up to $Z=51$, followed by a slight smooth decrease for higher Z elements. This decrease is a consequence of the progressive decrease of the autoionization branching ratios, due to the increase of the radiative transition coefficients, whereas the autoionization coefficients are approximately independent of Z. All the $3d^9 4s^2 5l$ configurations lie above the ionization limit for all the elements. The contributions of $3d$-$6l$ and $3d$-$7l$ are also displayed in Fig. 6, together with the total contribution from all the $3d$-nl ($n>7$) channels. The total contribution of all the extrapolated high-n channels is equal or smaller than that given by the $3d$-$6l$ channels.

Finally, the $3p$-$5l$ inner-shell excitations which involve high energy levels make a relatively small contribution to the total EA rate (Fig. 7). The $3p^5 3d^{10} 4s^2 5l$ configurations lie well above the first ionization limit throughout the sequence. As indicated above, one important autoionization channel is toward the Cu-like $3d^{10}5l$ excited levels. The $3p$-$5l$ EA processes are dominated by the $3p$-$5p$ inner-shell excitations. A noticeable drop occurs at $Z=55$ where a few levels fall below the $3d^{10}5l$ limit. Another decrease is observed around $Z=70$, where all the $3p$-$5l$ excited configurations lie below this limit. The discontinuities in the EA rates through $3p$-nl inner-shell excitations are unlike the EA behavior in the Cu sequence, in which the change in the EA rates is smooth, mostly dictated by the progressive change of the radiative decays compared to the autoionization rates. The sum of all the $3p$-nl EA channels for $n>5$ makes a total contribution close to that of the $3p$-$5l$ channel along the whole isoelectronic sequence.

In order to emphasize the effect of EA on the ionization balance in plasmas, it is convenient to introduce an effective enhancement factor of the collisional ionization rate coefficient due to the EA processes, defined by [4]:

$$R^{EA}\equiv\frac{(S+S^{EA})}{S}. \tag{3}$$

The ionization enhancement factor R^{EA} is shown in Fig. 8 for three temperatures $kT_e=0.3E_I$, $0.5E_I$, and E_I along the Zn sequence. The present results show that the effect of the EA processes is extremely important: for $Z=47$ at $kT_e=0.3E_I$ (which is close to the temperature T_{max} of maximum fractional abundance for this Zn-like ion in the coronal model [4]) R^{EA} reaches a value as high as 13. For comparison, the R^{EA} obtained in previous calculations [4] which take only the $3d$-$4l$ inner-shell excitations into account is also shown, for $kT_e=0.5E_I$. (One notices that the maximum in the $R^{EA}_{3d\text{-}4l}$ curve occurs for $Z=48$ instead of $Z=47$; this is due to the fact that mixing between configurations with different n was neglected in the previous computations.) For elements around $Z=55$, for which $kT_{max}\approx 0.5E_I$, the EA contribution of the additional high configurations causes the R^{EA} factor to increase by 80%. For lighter elements the increase is smaller: around $Z=43$ ($kT_{max}=0.3E_I$) R^{EA} increases by less than 30%. However, the introduction of the high $3d$-nl and $3p$-nl inner-shell excited configurations in the present revised EA calculations is crucial for elements with $Z>60$, since in this case the $3d$-$4l$ channels are completely closed. The relative importance of the additional EA channels is expected to progressively decrease for the following isoelectronic sequences (from GaI to KrI).

Finally, it is worth noting that the introduction of the multiple autoionization branching ratio model in the calculations has a small influence, which is less than 2% in the $48\leqslant Z\leqslant 60$ range. Outside this range, the usual approximate model which assumes no secondary autoionizations, i.e., $B_i^a=0$ [in Expression (1)] is practically equivalent to the present full model. Another simpler model, in which also $B_i^a=0$, but only the radiative decays to levels lying *below* the first ionization limit are included, has been also checked. The results show that this model would lead to an overestimation of the R^{EA} enhancement factor by about 10% for low Z elements, and up to 50% for the higher Z elements (this is due to the strong increase of the radiative decay rates as the ion charge increases). Consequently, this latter model appears not to be accurate enough.

TABLE II. Total rate coefficients S^{EA} for excitation-autoionization through all the $3d^{10}4s^2$-$3d^9 4s^2 nl$ and $3p^6 3d^{10}4s^2$-$3p^5 3d^{10}4s^2 nl$ inner-shell excitations in the Zn isoelectronic sequence. The coefficients are presented in the electron temperature range from 0.1 to 10 times the first ionization energy E_I and are given in $cm^3\ s^{-1}$ units. $X[-Y]$ means $X\times 10^{-Y}$.

					T_e			
Element	E_I (eV)	$0.1E_I$	$0.3E_I$	$0.5E_I$	$0.7E_I$	E_I	$2E_I$	$10E_I$
Se	65.6	5.98[-14]	1.97[-10]	9.97[-10]	1.96[-9]	3.20[-9]	5.32[-9]	6.19[-9]
Br	85.3	7.49[-14]	2.04[-10]	1.01[-9]	1.98[-9]	3.20[-9]	5.32[-9]	6.27[-9]
Kr	107.0	9.09[-14]	2.08[-10]	9.96[-10]	1.92[-9]	3.06[-9]	4.96[-9]	5.69[-9]
Rb	130.7	9.72[-14]	2.03[-10]	9.55[-10]	1.82[-9]	2.89[-9]	4.63[-9]	5.32[-9]
Sr	156.0	2.01[-13]	1.93[-10]	8.98[-10]	1.70[-9]	2.68[-9]	4.27[-9]	4.91[-9]
Y	183.4	1.11[-13]	1.93[-10]	8.67[-10]	1.62[-9]	2.52[-9]	3.97[-9]	4.54[-9]
Zr	212.7	1.27[-13]	1.90[-10]	8.36[-10]	1.54[-9]	2.37[-9]	3.68[-9]	4.17[-9]
Nb	243.7	1.38[-13]	1.86[-10]	7.95[-10]	1.45[-9]	2.22[-9]	3.39[-9]	3.81[-9]
Mo	276.6	1.51[-13]	1.81[-10]	7.52[-10]	1.36[-9]	2.06[-9]	3.12[-9]	3.48[-9]
Tc	311.3	1.25[-13]	1.59[-10]	6.66[-10]	1.20[-9]	1.83[-9]	2.79[-9]	3.14[-9]
Ru	347.9	1.17[-13]	1.47[-10]	6.09[-10]	1.10[-9]	1.66[-9]	2.52[-9]	2.85[-9]
Rh	386.6	1.23[-13]	1.41[-10]	5.72[-10]	1.02[-9]	1.53[-9]	2.31[-9]	2.59[-9]
Pd	427.0	1.31[-13]	1.35[-10]	5.38[-10]	9.49[-10]	1.42[-9]	2.12[-9]	2.37[-9]
Ag	469.1	1.37[-13]	1.30[-10]	5.06[-10]	8.87[-10]	1.31[-9]	1.95[-9]	2.16[-9]
Cd	513.2	6.75[-14]	9.07[-11]	3.77[-10]	6.75[-10]	1.02[-9]	1.56[-9]	1.82[-9]
In	559.1	7.13[-14]	8.71[-11]	3.52[-10]	6.27[-10]	9.43[-10]	1.43[-9]	1.66[-9]
Sn	607.0	7.62[-14]	8.42[-11]	3.34[-10]	5.88[-10]	8.79[-10]	1.32[-9]	1.52[-9]
Sb	657.2	7.82[-14]	7.94[-11]	3.09[-10]	5.42[-10]	8.04[-10]	1.20[-9]	1.37[-9]
Te	708.9	7.68[-14]	7.38[-11]	2.84[-10]	4.93[-10]	7.30[-10]	1.09[-9]	1.23[-9]
I	762.1	7.77[-14]	6.97[-11]	2.64[-10]	4.56[-10]	6.71[-10]	9.92[-10]	1.12[-9]
Xe	817.8	7.85[-14]	6.60[-11]	2.47[-10]	4.23[-10]	6.21[-10]	9.15[-10]	1.03[-9]
Cs	875.5	7.80[-14]	6.11[-11]	2.25[-10]	3.83[-10]	5.57[-10]	8.13[-10]	9.11[-10]
Ba	934.9	6.95[-14]	5.40[-11]	1.99[-10]	3.40[-10]	4.95[-10]	7.28[-10]	8.26[-10]
La	995.8	6.30[-14]	4.77[-11]	1.75[-10]	2.97[-10]	4.33[-10]	6.35[-10]	7.15[-10]
Ce	1058.8	6.01[-14]	4.41[-11]	1.60[-10]	2.73[-10]	3.99[-10]	5.86[-10]	6.63[-10]
Pr	1124.2	3.28[-14]	2.82[-11]	1.08[-10]	1.87[-10]	2.75[-10]	4.05[-10]	4.47[-10]
Nd	1191.5	3.18[-14]	2.62[-11]	9.88[-11]	1.70[-10]	2.50[-10]	3.67[-10]	4.04[-10]
Pm	1261.4	1.42[-14]	1.63[-11]	6.54[-11]	1.15[-10]	1.71[-10]	2.52[-10]	2.65[-10]
Sm	1332.6	1.46[-14]	1.56[-11]	6.15[-11]	1.08[-10]	1.60[-10]	2.34[-10]	2.46[-10]
Eu	1405.8	1.45[-14]	1.47[-11]	5.75[-11]	1.00[-10]	1.48[-10]	2.16[-10]	2.26[-10]
Gd	1481.3	1.44[-14]	1.36[-11]	5.21[-11]	8.99[-11]	1.31[-10]	1.89[-10]	1.97[-10]
Tb	1558.7	6.83[-15]	9.46[-12]	3.86[-11]	6.83[-11]	1.02[-10]	1.50[-10]	1.61[-10]
Dy	1637.6	6.71[-15]	8.88[-12]	3.59[-11]	6.32[-11]	9.39[-11]	1.38[-10]	1.47[-10]
Ho	1719.9	6.63[-15]	8.33[-12]	3.33[-11]	5.84[-11]	8.66[-11]	1.27[-10]	1.36[-10]
Er	1803.7	6.16[-15]	7.46[-12]	2.97[-11]	5.19[-11]	7.68[-11]	1.12[-10]	1.18[-10]
Tm	1888.9	5.91[-15]	6.74[-12]	2.64[-11]	4.60[-11]	6.79[-11]	9.83[-11]	1.03[-10]
Yb	1977.1	5.64[-15]	6.28[-12]	2.46[-11]	4.29[-11]	6.30[-11]	9.09[-11]	9.51[-11]
Lu	2067.8	5.21[-15]	5.62[-12]	2.20[-11]	3.82[-11]	5.59[-11]	8.07[-11]	8.41[-11]
Hf	2160.3	5.16[-15]	5.34[-12]	2.07[-11]	3.59[-11]	5.24[-11]	7.57[-11]	7.90[-11]
Ta	2254.3	4.75[-15]	4.83[-12]	1.87[-11]	3.22[-11]	4.72[-11]	6.79[-11]	7.09[-11]
W	2351.0	4.28[-15]	4.34[-12]	1.67[-11]	2.89[-11]	4.22[-11]	6.05[-11]	6.20[-11]
Re	2450.5	4.25[-15]	4.19[-12]	1.60[-11]	2.77[-11]	4.03[-11]	5.74[-11]	5.87[-11]
Os	2552.5	3.79[-15]	3.72[-12]	1.42[-11]	2.45[-11]	3.55[-11]	5.06[-11]	5.13[-11]
Ir	2656.5	3.60[-15]	3.45[-12]	1.31[-11]	2.25[-11]	3.28[-11]	4.65[-11]	4.72[-11]
Pt	2762.5	3.08[-15]	3.00[-12]	1.15[-11]	1.99[-11]	2.90[-11]	4.11[-11]	4.20[-11]
Au	2871.2	2.60[-15]	2.68[-12]	1.04[-11]	1.80[-11]	2.63[-11]	3.75[-11]	3.86[-11]
Hg	2981.9	2.61[-15]	2.57[-12]	9.93[-12]	1.71[-11]	2.49[-11]	3.54[-11]	3.62[-11]
Tl	3095.7	2.55[-15]	2.46[-12]	9.39[-12]	1.62[-11]	2.35[-11]	3.33[-11]	3.41[-11]
Pb	3211.6	1.37[-15]	1.82[-12]	7.32[-12]	1.28[-11]	1.90[-11]	2.76[-11]	2.90[-11]
Bi	3329.9	1.33[-15]	1.72[-12]	6.92[-12]	1.21[-11]	1.79[-11]	2.59[-11]	2.72[-11]
Po	3450.9	1.29[-15]	1.63[-12]	6.50[-12]	1.14[-11]	1.68[-11]	2.42[-11]	2.55[-11]
At	3574.6	1.17[-15]	1.51[-12]	6.05[-12]	1.06[-11]	1.57[-11]	2.26[-11]	2.39[-11]

TABLE II. (*Continued*).

Element	E_I (eV)	T_e $0.1E_I$	$0.3E_I$	$0.5E_I$	$0.7E_I$	E_I	$2E_I$	$10E_I$
Rn	3701.2	9.40[-16]	1.34[-12]	5.43[-12]	9.54[-12]	1.41[-11]	2.03[-11]	2.16[-11]
Fr	3829.6	9.21[-16]	1.27[-12]	5.13[-12]	9.01[-12]	1.33[-11]	1.92[-11]	2.03[-11]
Ra	3960.4	9.01[-16]	1.23[-12]	4.91[-12]	8.60[-12]	1.26[-11]	1.83[-11]	1.93[-11]
Ac	4095.6	8.81[-16]	1.17[-12]	4.66[-12]	8.14[-12]	1.20[-11]	1.72[-11]	1.82[-11]
Th	4232.3	8.63[-16]	1.11[-12]	4.41[-12]	7.70[-12]	1.13[-11]	1.62[-11]	1.71[-11]
Pa	4372.0	8.47[-16]	1.06[-12]	4.23[-12]	7.28[-12]	1.07[-11]	1.52[-11]	1.60[-11]
U	4515.7	8.32[-16]	1.02[-12]	4.04[-12]	6.87[-12]	1.01[-11]	1.43[-11]	1.50[-11]

C. Density range validity of the model

A collisional-radiative (CR) model [15] which assumes an optically thin plasma and includes all the $3d^{10}4s4l$ levels, was used for calculating the population of the low-lying levels along the whole isoelectronic sequence. These calculations were performed in order to define the electron density range of validity of the present model in which one has assumed collisional excitations from the ground state only, which in coronal conditions is the only level significantly populated. However, at higher electron-densities ionization (direct and EA) from excited configurations begins to be significant and must also be taken into account. One can define a critical electron density N_c, for which the total population of the first excited levels ($3d^{10}4s4p$) is equal, for instance, to 10% of the ground-state population.

In the Zn sequence, due to the presence of metastable levels ($4s4p\ ^3P_0$, $^3P_2$), the total population of the first excited levels is not negligible, even for a relatively low electron density, in contrast to the case of Cu-like ions [5]. The results of the CR population calculations show, for instance, that the critical density around the electron temperature of maximum fractional ion abundance is equal to 2×10^{14} cm^{-3} for Mo (at $kT_e\approx0.3E_I$), 5×10^{15} cm^{-3} for Xe (at $kT_e\approx0.5E_I$), and 2×10^{16} cm^{-3} for Au (at $kT_e\approx1.5E_I$). Due to the relatively low energy of the $3d^{10}4s4p$ levels compared to the ionization limit, the population of these levels is in fact not very sensitive to the temperature in the relevant range. At higher densities the contribution of EA processes from these excited levels may be significant. In order to evaluate this effect, the ratio between the rate coefficient for EA from the $3d^{10}4s4p$ ($^1P_1$, $^3P_{0,1,2}$) levels through the $3d$-$4l$ inner-shell excited configurations ($3d^9 4s4p4l$) and the direct-ionization rate coefficient S from the ground state (at $kT_e=E_I$), are calculated and shown in Fig 9, together with the ratio obtained for the $3d$-$4l$ EA processes from the ground state. Due to the high number of levels involved, the calculations have been performed without any configuration mixing (and for comparison, the EA rate from the ground state shown in the figure is also without $[4l+nl]$ configuration mixing). The results show that the rate coefficients for EA from the first excited levels are quite similar to those obtained for the ground state, in the low-Z range. In the high-Z range ($Z>58$) there is a discrepancy; however, this is not expected to have an important effect, since in this Z range the EA contributions of the $3d$-nl and $3p$-nl inner-shell excitations (not shown in Fig. 9) from the

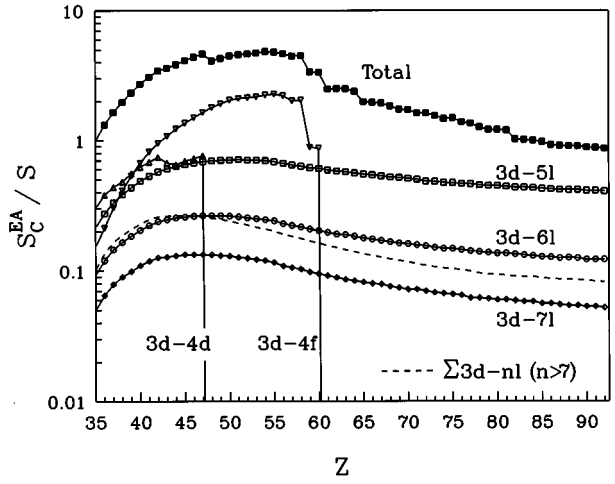

FIG. 6. Ratio of the excitation-autoionization rate coefficient S_C^{EA} to the direct-ionization rate coefficient S for the $3d$-$4d$, $3d$-$4f$, $3d$-$5l$, $3d$-$6l$, $3d$-$7l$, and $\Sigma 3d$-nl ($n>7$) inner-shell excitations, at an electron temperature equal to the first ionization energy E_I, as a function of the atomic number Z, along the Zn isoelectronic sequence. The ratio of the total S^{EA} rate coefficient to S is also displayed.

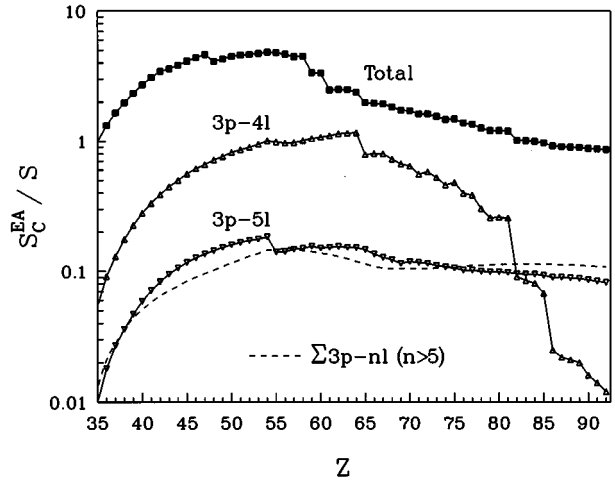

FIG. 7. Ratio of the excitation-autoionization rate coefficient S_C^{EA} to the direct-ionization rate coefficient S for the $3p$-$4l$, $3p$-$5l$, and $\Sigma 3p$-nl ($n>5$) inner-shell excitations, at an electron temperature equal to the first ionization energy E_I, as a function of the atomic number Z, along the Zn isoelectronic sequence. The ratio of the total S^{EA} rate coefficient to S is also displayed.

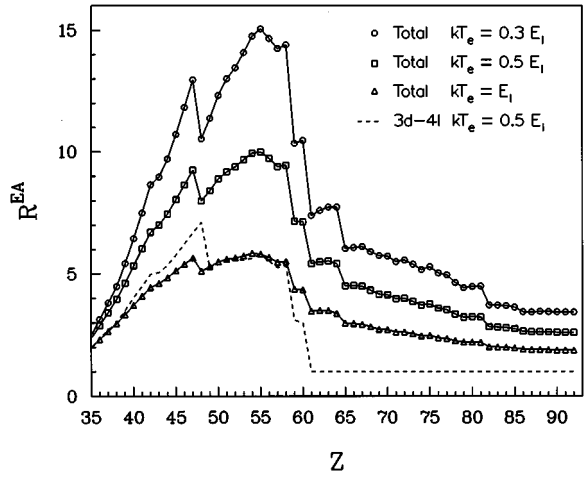

FIG. 8. Ratio R^{EA} of the total-ionization rate coefficient ($S^{EA}+S$) to the direct-ionization rate coefficient S, at an electron temperature equal to 0.3, 0.5 and 1 times the first ionization energy E_I, as a function of the atomic number Z, along the Zn isoelectronic sequence. For comparison, the ratio R^{EA} obtained in Ref. [4] by taking into account only the $3d$-$4l$ inner-shell excitations is also shown at $kT_e=0.5E_I$.

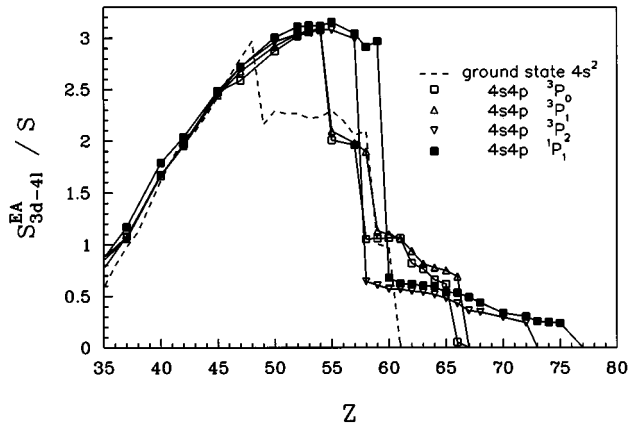

FIG. 9. Ratio between the rate coefficient $S^{EA}_{3d\text{-}4l}$ for excitation-autoionization from the first excited levels $3d^{10}4s4p$ ($^1P_1$, $^3P_{0,1,2}$) through $3d$-$4l$ inner-shell excitations (to $3d^9 4s4p4l$) and the rate coefficient S for direct-ionization from the ground state $3d^{10}4s^2\ ^1S_0$ (at $kT_e=E_I$), as a function of the atomic number Z, along the Zn isoelectronic sequence. For comparison, the ratio of the rate coefficient $S^{EA}_{3d\text{-}4l}$ for the ground state to S is also displayed.

ground state, and from the first excited levels as well, are dominant and are predicted to be similar.

In conclusion, even at an electron-density somewhat higher than N_c the present EA results may still be meaningful, since the EA rate coefficients for the ground and the low-lying levels are of the same order of magnitude.

V. CONCLUSIONS

We have shown the dominant role of the EA processes in the ionization mechanism all along the Zn isoelectronic sequence. Detailed calculations using the relativistic parameter potential and the distorted wave method were performed, enabling level-by-level computations of the EA cross sections and rate coefficients through the most important inner-shell excitations $3d$-nl ($n=4$ to 7) and $3p$-nl ($n=4,5$). These computations have been done for all the elements in the range $34\leqslant Z\leqslant 92$. The computations include radiative transitions among autoionizing levels, and further possible autoionization from these levels. The results show that neglecting further autoionizations leads to an error of 2% or less. Extrapolations for the $3d$-nl ($n>7$) and $3p$-nl ($n>5$) excitations were also included, leading to a contribution to the total EA rates varying from about 5% to 20% as Z increases along the sequence. The total contribution of the EA processes through the high-lying configurations, excited via $3d$-nl ($n\geqslant 5$) and $3p$-nl ($n\geqslant 4$), varies from 25% to 80% of the total EA effect in the $35\leqslant Z\leqslant 58$ range, whereas it constitutes the only EA mechanism for $Z\geqslant 61$.

Results of the EA cross section computations are presented for several Zn-like ions: Kr^{6+}, Mo^{12+}, Xe^{24+}, Pr^{29+}, and Dy^{36+}. In some cases, the EA processes enhance the total ionization cross section by more than one order of magnitude in a wide range of incident electron energies.

The present calculations predict that the EA processes in the Zn sequence increase the total ionization rate coefficient by a very large factor, varying from 3 to 13 in the range $35\leqslant Z\leqslant 47$ for $kT_e=0.3E_I$. This factor varies between 8 and 10 in the range $48\leqslant Z\leqslant 58$ for $kT_e=0.5E_I$, and decreases from 5 to 2 as Z increases up to 92 (for kT_e varying between E_I and $2E_I$).

These results show the particular importance of the EA effect in the fractional ion abundance modeling as a function of T_e in hot plasmas, such as in tokomaks, predicting a significant decrease in the temperature of maximum abundance, even larger than that calculated in our previous work [4].

ACKNOWLEDGMENTS

We are thankful to Professor M. Klapisch of the Naval Research Laboratories and Dr. W.H. Goldstein of the Lawrence Livermore National Laboratory for the use of the HULLAC atomic code package. We also thank E. Behar and R. Doron for fruitful discussions and their valuable comments.

[1] *Electron Impact Ionization*, edited by T.D. Märk and G.H. Dunn (Springer-Verlag, New York, 1985).
[2] K. Dolder, Adv. At. Mol. Opt. Phys. **32**, 69 (1994).
[3] D.L. Moores and K.J. Reed, Adv. At. Mol. Opt. Phys. **34**, 301 (1995).
[4] D. Mitnik, P. Mandelbaum, J.L. Schwob, J. Oreg, A. Bar-Shalom, and W.H. Goldstein, Phys. Rev. A **50**, 4911 (1994).
[5] D. Mitnik, P. Mandelbaum, J.L. Schwob, J. Oreg, A. Bar-Shalom, and W.H. Goldstein, Phys. Rev. A **53**, 3178 (1996).
[6] E. Behar, P. Mandelbaum, J.L. Schwob, A. Bar-Shalom, J.

Oreg, and W.H. Goldstein, Phys. Rev. A **52**, 3770 (1995).
[7] M. Klapisch, J.L. Schwob, B. Fraenkel, and J. Oreg, J. Opt Soc. Am. **67**, 148 (1977).
[8] J. Oreg, W.H. Goldstein, M. Klapisch, and A. Bar-Shalom, Phys. Rev. A **44**, 1750 (1991).
[9] A. Bar-Shalom, M. Klapisch, and J. Oreg, Phys. Rev. A **38**, 1733 (1988).
[10] K.J. LaGattuta and Y. Hahn, Phys. Rev. A **24**, 2273 (1981).
[11] P. Mandelbaum, J.F. Seely, A. Bar-Shalom, and M. Klapisch, Phys. Rev. A **44**, 5744 (1991).
[12] H. Van Regemorter, Astrophys. J. **136**, 906 (1962).
[13] W. Lotz, Z. Phys. **206**, 205 (1967); **216**, 241 (1968); **232**, 101 (1970).
[14] T.W. Gorczyca, M.S. Pindzola, N.R. Badnell, and D.C. Griffin, Phys. Rev. A **49**, 4682 (1994).
[15] D.R. Bates, F.R.S. Kingston, and R.W.P. McWhirter, Proc. R. Soc. A **267**, 297 (1962).